Catalysis Science & Technology

ROYAL SOCIETY OF CHEMISTRY

PAPER

View Article Online
View Journal | View Issue

Check for updates

Cite this: *Catal. Sci. Technol.*, 2025, **15**, 386

Characterizing Y224 conformational flexibility in FtmOx1-catalysis using ^{19}F NMR spectroscopy†

Xinye Wang,‡[a] Lingyun Yang,‡[b] Shenlin Wang,[a] Jun Wang,[c] Kelin Li,[d] Nathchar Naowarojna,[e] Yi Ju,[a] Ke Ye,[a] Yuchen Han,[a] Wupeng Yan,*[c] Xueting Liu,*[a] Lixin Zhang*[a] and Pinghua Liu*[d]

Received 8th September 2024,
Accepted 30th October 2024

DOI: 10.1039/d4cy01077a

rsc.li/catalysis

α-Ketoglutarate-dependent non-haem iron (αKG-NHFe) enzymes play a crucial role in natural product biosynthesis, and in some cases exhibiting multifunctional catalysis capability. This study focuses on αKG-NHFe enzyme FtmOx1, which catalyzes endoperoxidation, dealkylation, and alcohol oxidation reactions in verruculogen biosynthesis. We explore the hypothesis that the conformational dynamics of the active site Y224 confer the multifunctional activities of FtmOx1-catalysis. Utilizing Y224-to-3,5-difluorotyrosine-substituted FtmOx1, produced *via* the amber codon suppression method, we conducted ^{19}F NMR characterization to investigate FtmOx1's structural flexibility. Subsequent biochemical and X-ray crystallographic analyses provided insights into how specific conformations of FtmOx1–substrate complexes influence their catalytic activities. These findings underscore the utility of ^{19}F NMR as a powerful tool for elucidating the complex mechanisms of multifunctional enzymes, offering potential avenues for developing biocatalytic processes to produce novel therapeutic agents harnessing their unique catalytic properties.

1. Introduction

α-Ketoglutarate-dependent non-haem iron (αKG-NHFe) enzymes catalyze a wide range of reactions.[1–3] In recent years, there is a growing list of reports on multifunctional αKG-NHFe enzymes,[3,4] such as FtmOx1 (endoperoxidation, dealkylation, and alcohol dehydrogenation),[5–11] AusE (desaturation and spiro-ring-forming rearrangement),[12–14] PrhA (desaturation and cyclohepadiene formation),[13,14] AndA (desaturation and isomerization),[15,16] and DnmT (oxazoline formation, *N*-demethylation, and oxazoline decomposition).[17] The multifunctional nature of these enzymes adds a significant level of challenge in their mechanistic characterization and hinders further development for novel therapeutic agents using their unique catalytic properties.

FtmOx1, initially identified as an αKG-NHFe endoperoxidase in verruculogen biosynthesis,[18] is of particular interest due to the broad bioactivities of endoperoxides, such as antimalarial, antitumor, and antimicrobial properties.[8,19] Despite the importance of endoperoxides, there are only limited cases of reported endoperoxidases, including non-haem iron enzymes (FtmOx1[5,18] and NvfI[11]), haem-containing enzyme cyclooxygenase (COX),[20] and iodide peroxidase.[21] FtmOx1, an αKG-NHFe enzyme, was suggested to be an endoperoxidase catalysing endoperoxide installation between the C_{21} and C_{27} atoms of fumitremorgin B (**1**).[18] Subsequent studies further elucidates FtmOx1's catalytic complexity, demonstrating that it facilitates multiple reactions with fumitremorgin B (**1**) (Scheme 1):[5,7] (a) sequential endoperoxidation and alcohol oxidation of fumitremorgin B (**1**) to 13-oxoverruculogen (**3**) in the absence of a reductant; (b) dealkylation of fumitremorgin B (**1**) to produce 12,13-dihydroxyfumitremorgin C (**4**); (c) endoperoxidation of fumitremorgin B (**1**) to verruculogen (**2**) in the presence of a reductant; (d) dealkylation of 13-oxo-fumitremorgin B (**6**) to 12-hydroxy-13-oxo-fumitremorgin C (**7**).[7]

X-ray crystallographic characterization of FtmOx1 indicated that Y224 has more than one conformation in the FtmOx1 active site.[7] Such conformational flexibility was

[a] *State Key Laboratory of Bioreactor Engineering, East China University of Science and Technology, Shanghai 200237, China. E-mail: liuxueting@ecust.edu.cn, lizhang@ecust.edu.cn*
[b] *iHuman Institute, Shanghaitech University, Shanghai 201210, China*
[c] *School of Life Sciences and Biotechnology, Shanghai Jiao Tong University, Shanghai 200240, China. E-mail: yanwupeng@sjtu.edu.cn*
[d] *Department of Chemistry, Boston University, Boston, Massachusetts 02215, USA. E-mail: pinghua@bu.edu*
[e] *Program of Chemistry, Faculty of Science and Technology, Sakon Nakhon Rajabhat University, Sakon Nakhon 47000, Thailand*

† Electronic supplementary information (ESI) available: The mechanistic models proposed for FtmOx1, ^{19}F-NMR data, and crystallographic data. See DOI: https://doi.org/10.1039/d4cy01077a

‡ X. W. and L. Y. contributed equally to this work.

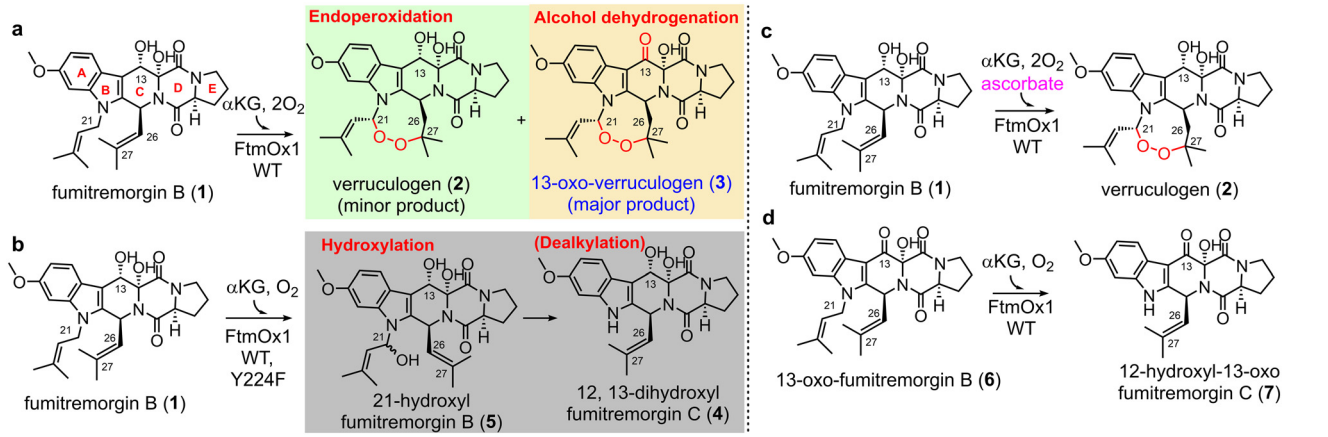

Scheme 1 Different reactions catalyzed by FtmOx1 and its variants under various conditions. (a) Endoperoxidation and alcohol oxidation in the absence of a reductant. (b) Dealkylation by WT-FtmOx1 and its variants. (c) Endoperoxidation in the presence of a reductant. (d) Dealkylation using the 13-keto analog as the substrate.

suggested to be a key to the multifunctional nature of the FtmOx1 enzyme.[5,6] To provide structural data for Y224 conformation flexibility in solution and more importantly, the correlation between Y224 conformation and catalysis, in this study, we replaced the active site tyrosine residue (Y224) with a fluorine-containing tyrosine analog 3,5-difluorotyrosine (F_2Y) and then we characterized the conformational changes of F_2Y224 using ^{19}F NMR spectroscopy.[22] The ^{19}F-atom has several unique features: (a) the ^{19}F atom has a spin 1/2 nucleus and a high gyromagnetic ratio, which results in a sensitivity as high as 83% compared to ^{1}H NMR; (b) the fluorine chemical shift range is ~100-fold wider than that of ^{1}H NMR, and ^{19}F NMR is sensitive to the changes in a local environment, which makes it an appropriate technique for probing active site conformations; (c) protein samples do not have ^{19}F NMR background signals, which makes ^{19}F NMR signals specific to the target of interest. Here, our ^{19}F NMR characterization of F_2Y224–FtmOx1 provides evidence for Y224 conformational flexibility. Subsequent X-ray crystallographic studies and biochemical data allow us to correlate Y224 conformations to various reactions catalyzed by FtmOx1.

2. Materials and methods

2.1. General

NMR spectra were acquired on a Varian NMR System (500 MHz for ^{1}H-NMR and 126 MHz for ^{13}C-NMR) and a Bruker BioSpin Avance III HD NMR spectrometer (600 MHz for ^{1}H NMR and 565 MHz for ^{19}F NMR). NMR spectra were recorded in 10% D_2O (99.9 atom% enriched, AICON) and 100 μM trifluoroacetic acid (TFA, 99.5 atom % enriched, Kanto). ^{19}F NMR chemical shifts were reported in δ values based on TFA (−76.20 ppm) as a reference. LC-HRMS-ESI measurements were performed on a Thermo Q Exactive Orbitrap mass spectrometer coupled with a Shimadzu LC-20 AD UPLC equipped with a Waters ACQUITY BEH C18 column (2.1 × 100 mm, 1.7 μm particles). Protein–substrate complexes were first screened for crystallization using a Crystal Gryphon auto dispenser (Art Robbins Instruments, LLC), and optimized crystals were sent to the Shanghai Synchrotron Radiation Facility (SSRF) to collect X-ray diffraction data under the beamline BL19U1 with a Pilatus3 6 M image plate detector. Biological reagents, chemicals, and media were purchased from standard commercial sources unless stated otherwise.

2.2. Overexpression and purification of tyrosine phenol lyase (TPL)

For protein overexpression, the pET22b vector harboring coding sequence of the TPL gene was transformed into *Escherichia coli* BL21 (DE3) cells (Invitrogen Inc., USA). A single colony was picked and placed into a Luria–Bertani (LB) medium supplemented with 100 μg mL^{-1} ampicillin and incubated at 37 °C overnight. 10 mL of the culture was inoculated in the 1 L LB medium supplemented with 100 μg mL^{-1} ampicillin. The culture was incubated at 37 °C until the OD_{600} reach 0.6–0.8 and then the TPL protein overexpression was induced by the addition of 0.2 mM isopropyl β-D-thiogalactoside at 18 °C for an additional 16 h before harvesting.

For protein purification, cells were suspended with the binding buffer (20 mM Na_2HPO_4, pH 8.0, 500 mM NaCl, 10 mM imidazole) and lysed by sonication (40 cycles of 3 s bursts) using a SCIENTZ IID ultrasonic processor followed by centrifugation at 4 °C for 60 min at 12 000 rpm. The supernatant was loaded onto the Ni-NTA column, followed by 10 column volution washing using washing buffer (20 mM Na_2HPO_4 pH 8.0, 500 mM NaCl, 20 mM imidazole). Then, the target protein was eluted with 10 column volume elution buffer (20 mM Na_2HPO_4 pH 8.0, 500 mM NaCl, 500 mM imidazole) and subjected to buffer exchange using Amicon stirred cells and 10 kDa ultrafiltration discs (Merck KGaA, Darmstadt, Germany). The desalting buffer used for buffer exchange contained 20 mM Na_2HPO_4 and 500 mM NaCl (pH 8.0).

2.3. Preparation of 3,5-difluorotyrosine (3,5-F_2Y)

The 3,5-F_2Y synthesis was done by following the reported procedures.[23] A 1 L reaction mixture contained 10 mM 2,6-difluorophenol, 30 mM ammonium acetate, 60 mM sodium pyruvate, 5 mM β-mercaptoethanol, 40 μM PLP, 50 mM KPi buffer (pH 8.0) and 40 mg of purified TPL protein. The reaction mixture was incubated in the dark with stirring at 25 °C for 4 days. Then, the reaction mixture was acidified to pH 3.0 with 6 M HCl and the precipitated protein was removed by celite filtration. The filtrate was extracted using 500 mL of ethyl acetate. The aqueous layer was loaded onto a 100 mL Dowex cation exchange column (Merck KGaA, Darmstadt, Germany). The column was washed with 500 mL of ACN : H_2O (3 : 7). 3,5-F_2Y was then eluted with a 6% ammonium hydroxide water solution. Fractions with the product were combined and lyophilized.

2.4. Overexpression and purification of F_2Y224–FtmOx1

The pASK-IBA3-plus-FtmOx1-Y224TAG variant construct was obtained using site-directed mutagenesis and confirmed using Sanger sequencing. For protein overexpression, the plasmids pASK-IBA3-plus-FtmOx1-Y224TAG and pEVOL-F_2YRS were co-transformed into *E. coli* BL21 (DE3) cells for protein overexpression. The engineered aminoacyl tRNA synthase F_2YRS[24] assisted the non-canonical amino acid 3,5-F_2Y insert at the specific site encoded by the nonsense codon TAG. A single colony was inoculated to an LB medium supplemented with 100 μg mL^{-1} ampicillin and 20 μg mL^{-1} chloramphenicol and incubated at 37 °C overnight. 100 mL of the culture was inoculated in 10 L of LB medium supplemented with 100 μg mL^{-1} ampicillin, 20 μg mL^{-1} chloramphenicol, and 0.1 mM ammonium ferrous sulfate. The culture was incubated at 37 °C until the OD_{600} reach ~0.8 and then F_2YRS was induced by adding arabinose up to 200 mg L^{-1} final concentration. When the OD_{600} reached ~1.2, the overexpression of F_2Y224–FtmOx1 was induced by the addition of anhydrotetracycline to a final concentration of 500 μg L^{-1} and added 3,5-F_2Y (1 mM). The culture was incubated at 20 °C for 12 h before harvesting by centrifugation.

In a typical anaerobic purification of F_2Y224–FtmOx1, ~10 g wet cell paste was resuspended in 50 mL of anaerobic buffer (100 mM Tris-HCl pH 7.5, 50 mM NaCl) in an anaerobic glove box. Lysozyme (5 mg mL^{-1} final concentration), EDTA (5 mM final concentration) and ascorbate (5 mM final concentration) were then added into the cell suspension, and the mixture was incubated on ice with gentle stirring for 30 min. The cells were disrupted by sonication (40 cycles of 3 s bursts) using a VCX130 ultrasonic processor. The supernatant and the cell debris were anaerobically separated by centrifugation at 4 °C for 60 min at 12 000 rpm. The resulting supernatant was mixed with 30 mL of Strep-Tactin resin (IBA Lifesciences GmbH, Göttingen, Germany) and incubated on ice for 30 min. Then, the column was washed with washing buffer (100 mM Tris-HCl pH 7.5, 50 mM NaCl) until the OD_{260} readout of the eluate was less than 0.05. The F_2Y224–FtmOx1 protein was eluted with elution buffer (2.5 mM desthiobiotin in 100 mM Tris-HCl pH 7.5 and 50 mM NaCl). The eluted protein was concentrated to be ~12 mg mL^{-1}, flash frozen with liquid nitrogen, and stored at −80 °C.

2.5. NMR experiments

NMR samples were prepared in an anaerobic glove box. The final concentration of the F_2Y224–FtmOx1, substrate (fumitremorgin B **1**/13-oxo-fumitremorgin B **6**), Zn^{II}, and αKG of different samples were 300 μM, 360 μM, 270 μM, and 600 μM, respectively. 500 μL solutions were pipetted into standard 5 mm O.D. NMR tubes containing 10% D_2O for NMR field-frequency lock and 100 μM TFA as an internal reference and a probe for magnetic field homogeneity.

NMR spectra were recorded at 298 K (600.13 MHz (^{1}H) and 564.93 MHz (^{19}F)) on a Bruker Avance III-HD spectrometer equipped with a 5 mm TCI ^{1}H/^{19}F–^{13}C–^{15}N probe with shielded Z-gradient coils. A typical fluorine NMR experiment included: spectrometer frequency = 565 MHz, temperature = 298.0 K, number of scans = 11 080–18 432, acquisition time = 0.5 s, relaxation delay = 1.0 s, pulse width = 12.3 μs, and receiver gain = 203 unless otherwise noted. The spectra were obtained using Bruker TOPSPIN, and the signals were deconvoluted with MestReNova software. The ^{19}F-chemical shifts were calibrated using an internal standard of TFA at −76.20 ppm.

2.6. Crystallization and data collection

The purified F_2Y224–FtmOx1 was incubated on ice for 15 min with Fe^{II} with a molar ratio of 1 : 3 to yield a final concentration of 6 mg mL^{-1}. F_2Y224–FtmOx1·Fe^{II} crystallization was set up using the sitting-drop vapor diffusion method by mixing protein and reservoir solution (100 mM MES pH 6.0, 50 mM $CoCl_2$, and 1.8 M ammonium sulfate) in a ratio of 2 : 1 at 20 °C. Sheet-like crystals were visible after 3 days.

The F_2Y224–FtmOx1 and αKG complex was obtained using both soaking and co-crystallization methods, which led to identical models. Crystal soaking was conducted by transferring the pre-formed F_2Y224–FtmOx1·Fe^{II} crystals into a crystallization reservoir solution containing 1 mM αKG and incubated for 6 h at room temperature. Co-crystallization was conducted by incubating F_2Y224–FtmOx1 with Co^{II} and αKG with a molar ratio of 1 : 3 : 3 to yield a final concentration of 10 mg mL^{-1}. Crystallization was carried out using the sitting-drop vapor-diffusion method by mixing the protein samples with an equal volume of reservoir solution at 20 °C. The best crystals of the binary complex were obtained in 100 mM Bis-Tris (pH 6.4), 50 mM $CoCl_2$, and 1.8 M ammonium sulfate. Plate-like crystals were visible after 5 days for the F_2Y224–FtmOx1·Co^{II}·αKG binary complexes.

Crystals were harvested for data collection and cryoprotected with a 25% (*v*/*v*) solution of glycerol mixed with

crystallization solution before being flash cooled in liquid nitrogen. Diffraction datasets were collected on the beamline BL19U1 at the Shanghai Synchrotron Radiation Facility (SSRF) at 100 K. Crystallographic datasets were integrated and scaled using HKL3000.[25] The crystal parameters and the data collection statistics are summarized in Tables S1 and S2.†

2.7. Structure determination and analysis

The F_2Y224–FtmOx1·Fe^{II} and F_2Y224–FtmOx1·Co^{II}·αKG crystals show a $P2_1$ space group with one homodimer per asymmetric unit, which is identical to the FtmOx1·Fe^{II} structure previously reported (bb entry 4Y5T). The structures of the F_2Y224–FtmOx1·Fe^{II} and F_2Y224–FtmOx1·Co^{II}·αKG complexes were solved by molecular replacement by Phaser as implemented in the Phenix/CCP4 suite,[26] using a model of FtmOx1·Fe^{II} structure (PDB entry 4Y5T). The initial solution was refined using phenix.refine, and the resulting 2m*F*o-D*F*c omit map showed clear electron density for the co-substrate αKG. The model was further improved using iterative cycles of manual model building in COOT,[27] followed by computational refinement using phenix.refine.[28,29] The positions of these automatically picked waters were checked manually during model building. Figures were generated with PyMOL.

2.8. Enzymatic reactions catalyzed by F2Y224–FtmOx1

The enzymatic reactions were performed in an anaerobic glove box. For the single-turnover condition, the anaerobic reaction mixture contained 63 μM fumitremorgin B (**1**) or 13-oxo-fumitremorgin B (**6**), 70 μM FtmOx1 containing 84 μM Fe^{II}, and 84 μM αKG. The reaction mixture was sealed and initiated by adding 200 μL of oxygen-saturated buffer (480 μM of oxygen in 100 mM Tris-HCl pH 7.5) and incubated for 10 min at room temperature. The enzymatic reactions were quenched by adding 1 mL dichloromethane, the precipitated protein was removed by centrifugation, and the dichloromethane layer was carefully separated for further analysis. The reaction mixture was extracted one more time using 1 mL of dichloromethane. The combined dichloromethane layers were concentrated by rotatory evaporation *in vacuo*. The resulting residue was then re-dissolved in 60 μL of acetonitrile and subjected to Q-TOF analysis using a C18 column (Waters ACQUITY BEH C18, 2.1 × 100 mm, 1.7 μm) with a flow rate of 0.35 mL min^{-1}. The mobile phase was a mixture of 0.1% HCOOH-containing H_2O and ACN, with the ACN concentration increasing from 5% to 60% over 9 minutes and then to 99% over the next 3 minutes (9–12 min). The column was subsequently eluted with 99% ACN in 0.1% HCOOH-containing H_2O for additional 3 minutes (12–15 min).

2.9. Circular dichroism (CD) spectroscopy

The F_2Y224–FtmOx1 apo protein was first buffer-exchanged into anaerobic 10 mM potassium phosphate buffer (pH 7.5) using Zeba™ Spin Desalting Columns (ThermoFisher). It was then reconstituted with 0.95 equivalents of Fe^{II} or Zn^{II} at room temperature for 10 minutes. The F_2Y224–FtmOx1 apo protein, F_2Y224–FtmOx1·Fe^{II}, and F_2Y224–FtmOx1·Zn^{II} were subsequently diluted to a final concentration of 0.35 mg mL^{-1} in anaerobic 10 mM potassium phosphate buffer (pH 7.5) within an anaerobic glove box. The CD spectra were collected using an Applied Photophysics CS/2 Chirascan. Spectra were recorded in the far-UV range (195–250 nm) using a quartz cuvette with a path length of 1 mm. A bandwidth of 1 nm and a scanning speed of 120 nm min^{-1} were used for data acquisition. The background spectra of the buffer were subtracted from the sample spectra to remove any contribution from the buffer. The CD data were expressed in terms of ellipticity (in mdeg).

3. Results and discussion

3.1. Incorporating unnatural amino acid 3,5-F_2Y into FtmOx1

To site-specifically replace Y224 in the FtmOx1 active site with 3,5-F_2Y, the amber codon suppression method was employed.[24,30] The Y224 codon in FtmOx1 was substituted with the amber stop codon TAG and co-expressed with the F_2Y tRNA-synthetase pair in a culture medium supplemented with 3,5-F_2Y, as previously described (Fig. 1a–e).[31] The F_2Y224–FtmOx1 protein was purified anaerobically as in previous studies.[5–7] The incorporation of 3,5-F_2Y was confirmed by mass spectrometric analysis, which showed an observed average mass of 35704.96 Da for F_2Y224–FtmOx1, 36.94 Da larger than that for WT-FtmOx1 with an average mass of 35668.02 Da (Fig. 1d). To further confirm the site-specific incorporation, tryptic digested peptides of F_2Y224–FtmOx1 were characterized by tandem mass spectrometry (Fig. 1e), revealing the incorporation of 3,5-F_2Y at the 224 position of FtmOx1.

3.2. ^{19}F NMR analysis of F_2Y224 conformation

FtmOx1 is an αKG-NHFe endoperoxidase[18] with multifunctional activities that can be modulated by various substrate analogs.[7] Previous studies have shown that Y224 adopts two different conformations.[5–7] However, the relationship between Y224's conformational changes under different reaction conditions and its impact on enzymatic activity remains unclear. To address these questions, we performed ^{19}F NMR analysis of F_2Y224–FtmOx1 and revealed a single peak at δ = −133.41, suggesting a single conformational state of F_2Y224 in the apo-protein or multiple conformations in quick equilibrium (Fig. 2-i).

Previous crystallographic studies of FtmOx1 reveal that the distance between the hydroxyl group of Y224 and the metallo-center varies between 4.4 Å and 8.8 Å, depending on Y224's conformation (PDB entries 4Y5T and 7WSB).[5,7] At these distances, ^{19}F NMR signal intensities and relaxation properties are likely to be influenced by the presence of the metallocenter.[32,33] To test this hypothesis, we reconstituted apo-FtmOx1 with several common first row transition metal

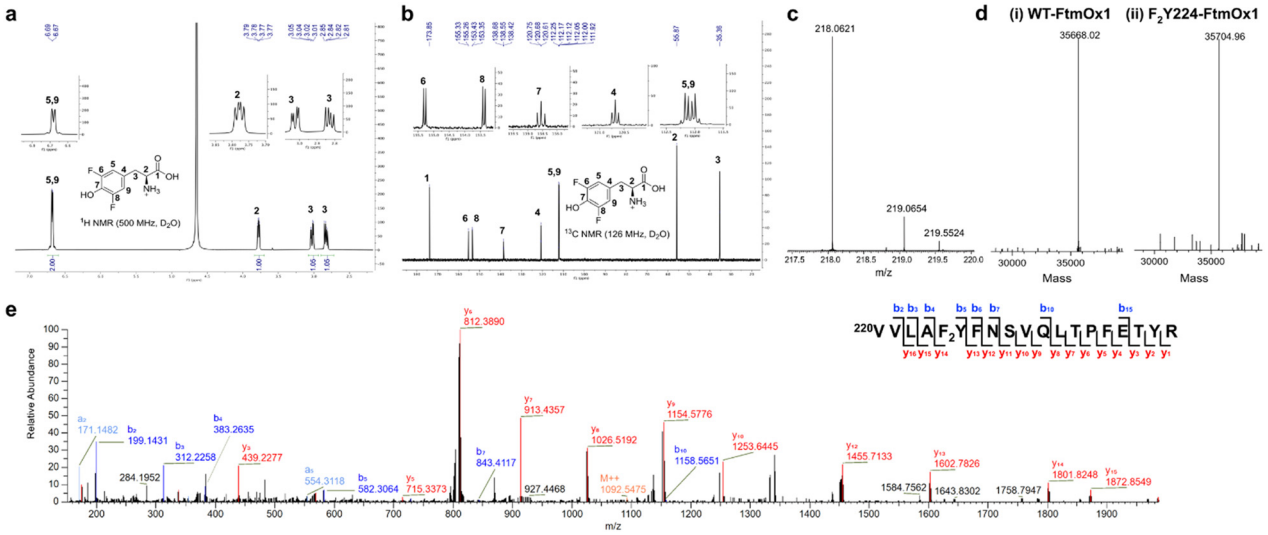

Fig. 1 Characterization of 3,5-difluorotyrosine (3,5-F_2Y) and F_2Y224–FtmOx1. (a) ^{1}H-NMR spectrum of 3,5-F_2Y. (b) ^{13}C-NMR spectrum of 3,5-F_2Y. (c) MS spectrum of 3,5-F_2Y. Calculated *m/z* for 3,5-F_2Y ($[M + H]^+$ form, positive mode) was 218.0623 and found at 218.0621. (d) ESI-MS spectra of WT-FtmOx1 (i) and F_2Y224–FtmOx1 (ii). (e) MS/MS spectrum of the tryptic peptides of F_2Y224–FtmOx1. The peptide fragment (residue 220 to residue 237) with $[M + H]^{2+}$ of 2182.0881 (predicted *m/z*: 2182.0909) identified the 3,5-F_2Y residue at position 224, which suggests the successful incorporation of 3,5-F_2Y at position 224 in FtmOx1.

ions, including Fe^{II}, Co^{II}, Ni^{II}, and Zn^{II} and then characterized them using ^{19}F NMR (Fig. S1†). Consistent with literature information,[32–34] in the presence of a paramagnetic center, such as Fe^{II}, Co^{II}, or Ni^{II}, the local paramagnetic relaxation enhancement (PRE) significantly increases the relaxation rate constants of nearby ^{19}F, and results in the quenching of the ^{19}F NMR signal. Strong ^{19}F NMR signals were observed when apo-FtmOx1 was reconstituted using the diamagnetic Zn^{II} ion (Fig. S1† and 2-ii). No overall structure perturbation of the enzyme was observed in the CD spectrum when replacing Fe^{II} with Zn^{II} (Fig. S2†). Three signals (δ −128.83, −130.85, and −135.08) were observed in the ^{19}F NMR spectrum of Zn^{II}-reconstituted F_2Y224–FtmOx1, which suggests that F_2Y224 in FtmOx1 indeed adopts multiple conformations.

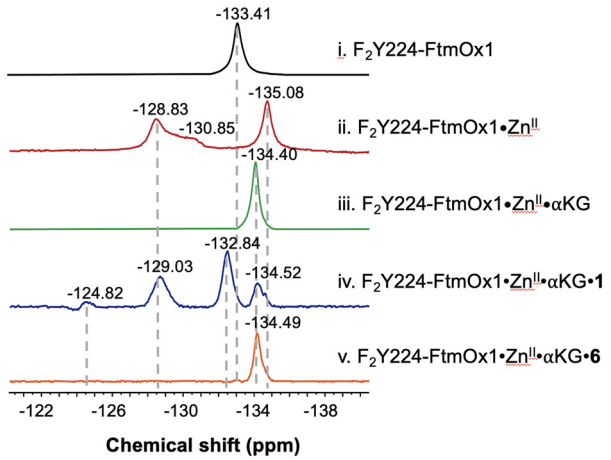

Fig. 2 ^{19}F-NMR experiments using fumitremorgin B (**1**) and 13-oxo-fumitremorgin B (**6**) as the substrates. ^{19}F NMR spectra of F_2Y224–FtmOx1 incubated with (i) apo protein, (ii) Zn^{II}, (iii) Zn^{II} and αKG, (iv) Zn^{II}, αKG, and **1**, and (v) Zn^{II}, αKG, and **6**.

Encouraged by this result, we further characterized the F_2Y224–FtmOx1·Zn^{II}·αKG binary complex using ^{19}F NMR. The complex was prepared by mixing F_2Y224–FtmOx1, Zn^{II} ions, and αKG in a ratio of 1 : 0.9 : 2. Interestingly, the ^{19}F NMR spectrum of the F_2Y224–FtmOx1·Zn^{II}·αKG binary complex shows a single dominant signal at δ = −134.40 (Fig. 2-iii), indicating that the presence of αKG significantly stabilizes one specific protein conformation. In our prior report on the crystal structures of Fe^{II}-containing FtmOx1 and the FtmOx1·Fe^{II}·αKG binary complex (PDB entries 4Y5T and 4Y5S),[5] Y224 was positioned similarly in both structures, forming a hydrogen bond with a water ligand of the metallo-center with the distances between the hydroxyl group of Y224 and two oxygen atoms of the αKG 1-carboxyl group being ~3.4 Å and 4.3 Å (Fig. S3†), respectively. This result suggests that in the FtmOx1·Fe^{II}·αKG binary complex, Y224 may form hydrogen bonds with both the 1-carboxyl group of αKG and the metallo-center water ligand.

The presence of three distinct ^{19}F NMR signals in the F_2Y224–FtmOx1·Zn^{II} complex (δ −128.83, −130.85, and −135.08) indicates that FtmOx1 exists in multiple conformations in solution with the conformation observed in the FtmOx1·Fe^{II} structure (PDB entry 4Y5T) being one of them. Notably, relative to one dominant ^{19}F NMR signal at δ −133.41 in apo-F_2Y224–FtmOx1, the chemical shifts of one of the signals in F_2Y224–FtmOx1·Zn^{II} at δ = −135.08 and the signal in F_2Y224–FtmOx1·Zn^{II}·αKG at δ = −134.40 are different (Fig. 2ii and iii). If these signals are all associated with one Y224 conformation, the differences in ^{19}F NMR

chemical shifts suggest that ^{19}F NMR is sensitive to changes in the enzyme active site environment and is a suitable tool to study protein conformational changes.

To further probe the dynamic states of Y224 in the presence of the substrate, we performed ^{19}F NMR analysis of the F_2Y224–FtmOx1·Zn^{II}·αKG·**1** ternary complex and revealed four signals (δ = −124.82, −129.03, −132.84, and −134.52), which differ from those of the F_2Y224–FtmOx1·Zn^{II}·αKG binary complex. Notably, replacing the substrate fumitremorgin B (**1**) with the substrate analog 13-oxo-fumitremorgin B (**6**) leads to a single peak (δ −134.49) for the F_2Y224–FtmOx1·Zn^{II}·αKG·**6** ternary complex (Fig. 2-v). Such a significant difference in solution ^{19}F NMR spectra raises an immediate question: what are the activities of F_2Y224–FtmOx1 under various conditions and the correlation between F_2Y224–FtmOx1 solution conformations, the F_2Y224–FtmOx1 activities, and the X-ray crystal structures?

3.3. Biochemical characterization of F_2Y224–FtmOx1

To correlate structural observations with enzymatic activity, we performed single-turnover reactions on WT-FtmOx1 and the mutant F_2Y224–FtmOx1 using different setups: (a) with fumitremorgin B (**1**) as the substrate without additional reductants; (b) with fumitremorgin B (**1**) and excess ascorbate as the reductant; (c) with 13-oxo-fumitremorgin B (**6**) as the substrate. As shown in Fig. 3, WT-FtmOx1 and F_2Y224–FtmOx1 shares similar biochemical properties. Using the fumitremorgin B (**1**) substrate without extra reductants, both enzymes primarily produce 13-oxo-verruculogen (**3**) as the major product and verruculogen (**2**) as the minor product under single-turnover conditions (traces i and ii, Fig. 3b).

This result suggests that in the absence of extra reductants (*e.g.*, ascorbate), WT-FtmOx1 and F_2Y224–FtmOx1 catalyze a sequential endoperoxidation and alcohol oxidation reactions (**1** → **2** → **3**, Fig. 3a-I). The HPLC profiles of both WT-FtmOx1 and F_2Y224–FtmOx1 catalyzing the reaction mixture show that 13-oxo-verruculogen (**3**) is the predominant product, with a production ratio of 5 : 1 and 5 : 2 over verruculogen (**2**), respectively. The minor dealkylation products (**4** & **7**) appear at low levels, with an endoperoxidation to dealkylation ratio shifting from 4 : 1 in WT-FtmOx1 to 7 : 3 in F2Y224–FtmOx1 (traces i & ii in Fig. 3b). This initial study using fumitremorgin B (**1**) suggests that the Y224 to F2Y224 substitution does not significantly alter the catalysis of FtmOx1 under single-turnover conditions in the absence of a reductant.

In the presence of ascorbate, WT-FtmOx1 primarily produces verruculogen (**2**) being the dominant product (Fig. 3a-II and trace iii in Fig. 3b).[5–7] However, in reactions involving the F_2Y224–FtmOx1 mutant, adding ascorbate alters the production ratio of compounds **2** and **3** to nearly equal levels (trace iv in Fig. 3b). The incorporation of F_2Y224 in FtmOx1 seems to mitigate the effect of ascorbate on the alcohol dehydrogenation step in the enzyme's catalysis. This result suggests that ascorbate specifically impacts the latter stages of the sequential **1** → **2** → **3** reaction, with no apparent effect on the initial endoperoxidation step.

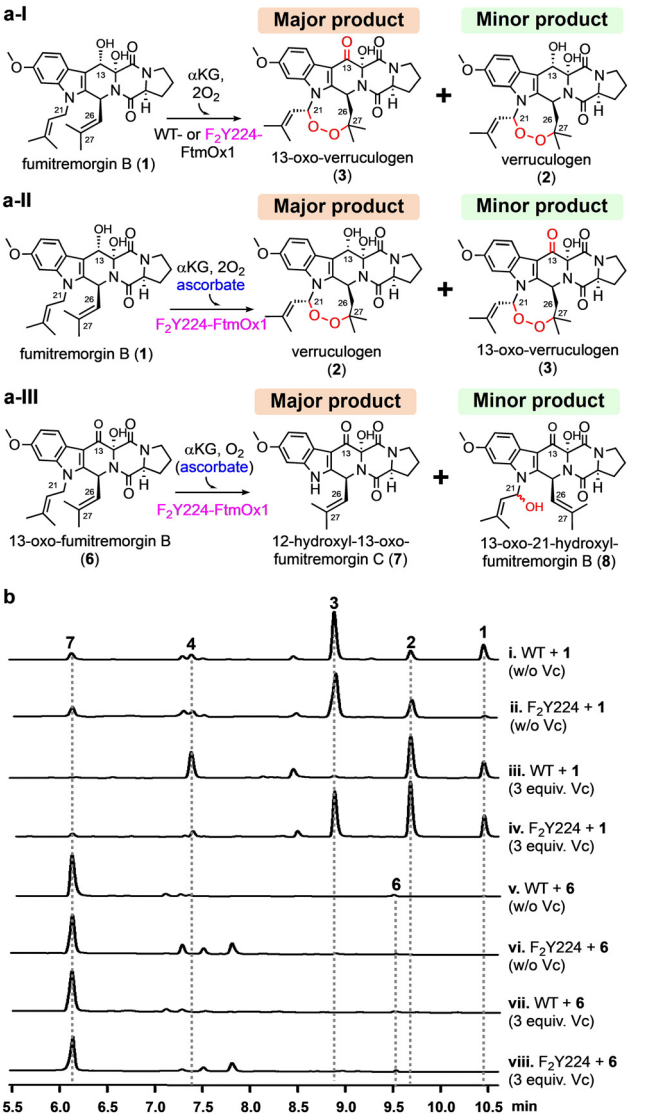

Fig. 3 Biochemical reactions catalyzed by the WT-FtmOx1 and the F_2Y224–FtmOx1 mutant using fumitremorgin B (**1**) and 13-oxo-fumitremorgin B (**6**) as the substrates. (a) Different FtmOx1-catalysis outcomes under slightly different conditions observed for the WT-FtmOx1 and the F_2Y224–FtmOx1 mutant: (a-I) under non-reducing condition (without ascorbate), both WT-FtmOx1 and F_2Y224–FtmOx1 react with fumitremorgin B (**1**) to primarily produce 13-oxo-verruculogen (**3**) as the major product and verruculogen (**2**) as the minor product; (a-II) under reducing condition (with ascorbate), F_2Y224–FtmOx1 reacts with fumitremorgin B (**1**) to primarily produce verruculogen (**2**) as the major product and 13-oxo-verruculogen (**3**) as the minor product. (a-III) with 13-oxo-fumitremorgin B (**6**) as the substrate for F_2Y224–FtmOx1 reaction, the dealkylation product 12-hydroxyl-13-oxo-fumotremorgin C (**7**) is the dominant product; (b) HPLC profiles (i–viii) of reactions under single-turnover conditions from the WT-FtmOx1 and the F_2Y224–FtmOx1 mutant. The reaction mixture contains enzyme (70 μM), Fe^{II} (84 μM), fumitremorgin B (63 μM), αKG (84 μM), and O_2 (480 μM).

When 13-oxo-fumitremorgin B (**6**) was used as the substrate, the HPLC profiles of the products in F_2Y224–FtmOx1-catalysis (trace vi in Fig. 3b) closely resemble those of WT-FtmOx1-catalysis (trace v in Fig. 3b). In both cases, the dealkylation product 12-hydroxyl-13-oxo-fumitremorgin C (**7**) is the

dominant product and the presence or absence of ascorbate does not alter the product profile (Fig. 3a-III, traces vi & viii in Fig. 3b). These biochemical characterization results indicate that F2Y224–FtmOx1 retains all three essential reactions reported for WT-FtmOx1 (Fig. 3a). Therefore, F_2Y224 substitution represents a suitable system to study the conformation of Y224 in solution for FtmOx1-catalysis.

3.4. Structural characterization of F_2Y224–FtmOx1

^{19}F NMR is very sensitive to environmental changes and is an excellent tool to study protein conformational changes. However, correlating ^{19}F NMR signals to structural information has been challenging. In this particular case, both the ^{19}F NMR spectrum (Fig. 2) and the catalytic reaction of F_2Y224–FtmOx1 for substrate analog **6** is relatively clean (Fig. 3a-III), which could serve as a reasonable starting point for correlating the ^{19}F NMR signals to structural information. In addition, consistent with complicated reaction outcomes for substrate **1**, the ^{19}F-NMR spectrum indicated the presence of multiple conformations. Besides ^{19}F-NMR studies, we also solved the crystal structures for F_2Y224–FtmOx1·Fe^{II} complex (PDB entry 9J1I) at a resolution of 2.1 Å. The overall architecture of this complex is analogous to those of FtmOx1·Fe^{II} (PDB entry 4Y5T) and FtmOx1·Fe^{II}·αKG (PDB entry 4Y5S) (Fig. S4†), which provides additional evidence suggesting that F_2Y224–FtmOx1 could serve as a good surrogate for WT-FtmOx1 in studying Y224 conformations. F_2Y224–FtmOx1 exists as a dimer (Fig. 4a) and the dimer is formed by an internal twofold symmetry operator, with each active site generated by residues from both monomers. In the F_2Y224–FtmOx1·Fe^{II} structure, H129, D131, and H205, together with three well-ordered water molecules, form an approximate octahedral coordination around the mononuclear iron (Fig. 4b and S5†). Superimposition of the F_2Y224–FtmOx1·Fe^{II} structure onto FtmOx1·Fe^{II} (PDB entry 4Y5T) revealed that the unnatural amino acid residue Y224F_2Y slightly rotates around the C_β–C_γ bond by ~33° compared to the residue Y224 in WT-FtmOx1 (Fig. 4c). The metallo-center water ligand *trans* to H129 forms a hydrogen bond with the F_2Y224 hydroxyl group. The distance between the F_2Y224 hydroxyl group and the mononuclear iron center is ~4.3 Å, which is similar to that in WT-FtmOx1 (~4.4 Å).

Despite extensive efforts, we could not obtain the co-crystallization of F_2Y224-FtmOx1 with αKG. Therefore, we have attempted soaking αKG into F_2Y224–FtmOx1·Fe^{II} crystals or F_2Y224–FtmOx1·Co^{II} crystals. Through these efforts, F_2Y224–FtmOx1·Fe^{II}·αKG at a resolution of 2.8 Å and F_2Y224-FtmOx1·Co^{II}·αKG (PDB entry 9J1H) at a resolution of 2.0 Å have been obtained. Superimposing the structures of the F_2Y224–FtmOx1·Fe^{II}·αKG (2.8 Å) complex onto the F_2Y224–FtmOx1·Co^{II}·αKG (2.0 Å) complex indicated a good alignment of their backbone (RMSD < 0.4 Å) and similar side chain orientations of metallo-center (Fig. S6†). In the F_2Y224–FtmOx1·Co^{II}·αKG binary complex, the αKG molecule binds to the iron center in a bidentate fashion (Fig. 4d), and the αKG 1-carboxylate group binds *trans* to H205, exhibiting a distal-type binding mode, which is similar to the FtmOx1·Fe^{II}·αKG binary complex structure (PDB entry 4Y5S). Interestingly, in the F_2Y224–FtmOx1·Co^{II}·αKG binary (PDB entry 9J1H) complex, the loop region (^{65}ADKYPPHF^{72}) which is proposed to be re-arranged during the binding of substrate fumitremorgin B (**1**) or 13-oxo-fumitremorgin B (**6**) shows a different conformation between chain A and chain B (Fig. S7a†). The loop region of chain A is close to 7WSB (substrate binding state) (Fig. S7b†),[7] while that of chain B is consistent with 4Y5S (αKG binding state) (Fig. S7c†).[5] In the reaction reported in Fig. 3, we indeed noticed that for the sequential **1** → **2** → **3** reaction, Y_2Y224–FtmOx1 does behave slightly

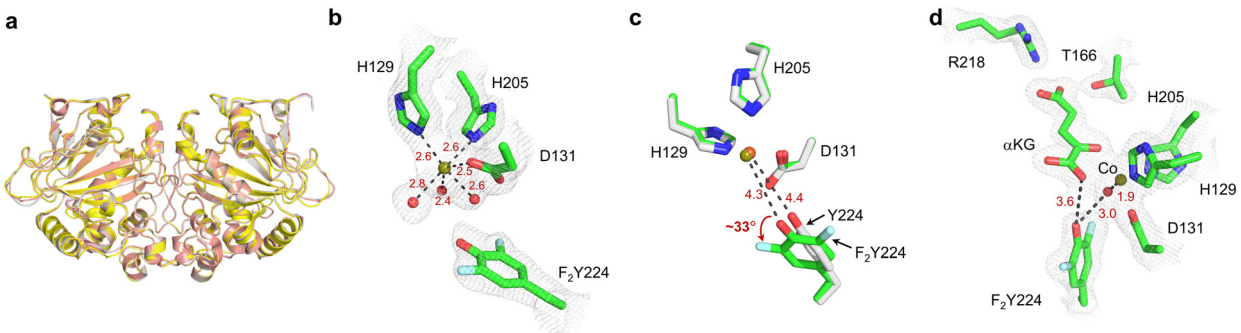

Fig. 4 Structures of the F_2Y224–FtmOx1 mutant. (a). Superimposition of the F_2Y224–FtmOx1·Fe^{II} (PDB entry 9J1I) structure with FtmOx1·Fe^{II} (PDB entry 4Y5T) and FtmOx1·Fe^{II}·αKG (PDB entry 4Y5S) structures. The F_2Y224–FtmOx1·Fe^{II} structure is shown in yellow. The FtmOx1·Fe^{II} structure is shown in grey. The FtmOx1·Fe^{II}·αKG structure is shown in pink. (b). The omit map of the F_2Y224–FtmOx1 metallo-center (2m*Fo*-D*Fc*) at 1σ contour. The map was generated by phenix using simple refinement after omitting each region. The electron density around each compound is shown in grey mesh. The residues coordinating with the metallo-center are shown as sticks. The coordination of iron is represented by dashed lines. (c). Superimposition of F_2Y224–FtmOx1·Fe^{II} metallo-center (PDB entry 9J1I) with FtmOx1·Fe^{II} (PDB entry 4Y5T). The F_2Y224–FtmOx1 metallo-center is shown in green. The FtmOx1·Fe^{II} metallo-center is shown in grey. (d). F_2Y224–FtmOx1·Co^{II}·αKG binary (PDB entry 9J1H) complex. The omit map of the metallo-center and αKG (2m*Fo*-D*Fc*) at 1σ contour. The electron density around each compound is shown in grey mesh. The residues within 4 Å around the αKG are shown as stick. The distances between Y224F_2Y and the αKG and the metallo-center are highlighted with black dashed lines.

differently from WT-FtmOx1, especially the **2** → **3** part, which might be related to the slight differences in the loop region. Another important feature observed in these crystal structures is that, in the F_2Y224–FtmOx1·Co^{II}·αKG complex, F_2Y224 is H-bonded to the metallo-center water ligand (Fig. S7a†), similar to what has been observed in the FtmOx1·Co^{II}·αKG binary complex. Consistent with the existence of multiple conformations for F_2Y224, our efforts on obtaining the F_2Y224–FtmOx1·Fe^{II}·αKG·**1** complex failed. In the future, we might need to explore methods to selectively stabilize one of the conformations to help structural studies for F_2Y224–FtmOx1·Fe^{II}·αKG·**1** and FtmOx1·Fe^{II}·αKG·**1** complexes to increase our chance of obtaining high quality crystals.

4. Conclusions

Herein, we reported the biochemical and ^{19}F NMR characterization of FtmOx1-catalysis using F_2Y224–FtmOx1. Recent studies employing unnatural tyrosine incorporation in FtmOx1 catalysis have revealed significant challenges.[35,36] Specifically, Lin *et al.* reported difficulties in purifying fluorotyrosine-substituted FtmOx1 at the Y224 position, resulting in a lack of biochemical or structural data regarding this mutant.[35] Similarly, Wang *et al.* successfully obtained soluble F_2Y224–FtmOx1 protein; however, purification under aerobic conditions led to a complex mixture of reaction products, precluding effective structure–function correlation analysis.[36] Our research aims to address these gaps. Previous work has established that FtmOx1 catalysis is complex and outcomes are highly sensitive to numerous factors including protein purification conditions, reaction conditions, substrate analog structures, and the conformational state of the active site tyrosine Y224.[5,7] To overcome these challenges, we overexpressed and purified F_2Y224–FtmOx1 under anaerobic conditions, mirroring the methodology applied in our studies with wild-type FtmOx1.

^{19}F NMR analysis indicated that the F_2Y224–FtmOx1·Zn^{II}·αKG·**1** ternary complex might have multiple conformations with four signals (δ −124.82, −129.03, −132.84 and −134.52) in the ^{19}F NMR spectrum. Such conformational flexibility in solution is also consistent with the complicated sequential **1** → **2** → **3** transformations. In contrast, the ^{19}F NMR spectrum of the F_2Y224–FtmOx1·Zn^{II}·αKG·**6** ternary complex has one predominant ^{19}F NMR signal (δ −134.49). The biochemical characterization of the F_2Y224–FtmOx1 catalyst using compound **6** indicated that the product is the result of a dealkylation reaction and barely has other reactions. The solution conformational information on F_2Y224–FtmOx1 is fully consistent with the biochemical data, implying the important role of Y224 in FtmOx1-catalysis.[5,7]

The structural information in solution was also consistent with the recent X-ray structural information.[7,9] In WT-FtmOx1, it has been challenging to obtain the structure of the ternary complex and one of the structures obtained is correlated with the dealkylation reaction.[7,9] As a complementary method to X-ray structural studies, ^{19}F NMR spectroscopy is well-suited for characterizing such complexes with a highly dynamic nature, and paves the way for future detailed characterization of these Y244 conformations and factors governing these conformational changes. With more and more cases of multifunctional αKG-NHFe enzymes,[3,4] a combination of solution structural information, biochemical data, and X-ray structural data will provide more comprehensive information on how various activities of these multi-function enzymes are modulated.

Data availability

The crystallographic data are provided in the ESI.† All other data underlying this work will be shared on reasonable request to the corresponding authors.

Author contributions

P. L., L. Z., X. L., and W. Y. designed the study. X. W., L. Y., and S. W. performed the ^{19}F NMR experiments and data analysis. X. W., J. W., and W. Y. performed the crystallization and structural determination. Y. J., K. Y., Y. H., and K. L. performed the synthetic and biochemical experiments. X. W., W. Y., X. L., K. L., N. N., and P. L. analyzed the data and wrote the manuscript with input from all authors. All authors have given approval for the final version of the manuscript.

Conflicts of interest

There are no conflicts to declare.

Acknowledgements

This work was supported by the National Key Research and Development Program of China (2020YFA0907800 and 2022YFC2105400), the National Natural Science Foundation of China (22307037, 31720103901, 21977029, 81903529, and 32101008), the Open Project Funding of the State Key Laboratory of Bioreactor Engineering, and the 111 Project (B18022). This work was supported in part by the National Institutes of Health (GM140040 to P. L.). The authors thank the staff members at the BL02U1 and BL19U1 beamline at the Shanghai Synchrotron Radiation Facility (SSRF), China, for their assistance in X-ray crystal data collection. A CD spectrometer was provided by NSF MRI grant CHE-112654.

References

1 H. Nakamura, Y. Matsuda and I. Abe, Unique chemistry of non-heme iron enzymes in fungal biosynthetic pathways, *Nat. Prod. Rep.*, 2018, **35**(7), 633–645.
2 R. Ushimaru and I. Abe, Unusual Dioxygen-Dependent Reactions Catalyzed by Nonheme Iron Enzymes in Natural Product Biosynthesis, *ACS Catal.*, 2023, **13**(2), 1045–1076.

3 S.-S. Gao, N. Naowarojna, R. Cheng, X. Liu and P. Liu, Recent examples of α-ketoglutarate-dependent mononuclear non-haem iron enzymes in natural product biosyntheses, *Nat. Prod. Rep.*, 2018, **35**(8), 792–837.
4 T. Awakawa, T. Mori, R. Ushimaru and I. Abe, Structure-based engineering of α-ketoglutarate dependent oxygenases in fungal meroterpenoid biosynthesis, *Nat. Prod. Rep.*, 2023, **40**(1), 46–61.
5 W. Yan, H. Song, F. Song, Y. Guo, C. H. Wu, A. S. Her, Y. Pu, S. Wang, N. Naowarojna, A. Weitz, M. P. Hendrich, C. E. Costello, L. Zhang, P. Liu and Y. J. Zhang, Endoperoxide formation by an alpha-ketoglutarate-dependent mononuclear non-haem iron enzyme, *Nature*, 2015, **527**(7579), 539–543.
6 W. Yan, H. Song, F. Song, Y. Guo, C.-H. Wu, A. S. Her, Y. Pu, S. Wang, N. Naowarojna, A. Weitz, M. P. Hendrich, C. E. Costello, L. Zhang, P. Liu and Y. J. Zhang, Retraction Note: Endoperoxide formation by an α-ketoglutarate-dependent mononuclear non-haem iron enzyme, *Nature*, 2021, **593**(7860), 612.
7 G. Zhu, W. Yan, X. Wang, R. Cheng, N. Naowarojna, K. Wang, J. Wang, H. Song, Y. Wang, H. Liu, X. Xia, C. E. Costello, X. Liu, L. Zhang and P. Liu, Dissecting the Mechanism of the Nonheme Iron Endoperoxidase FtmOx1 Using Substrate Analogues, *JACS Au*, 2022, **2**(7), 1686–1698.
8 N. P. Dunham, J. M. Del Río Pantoja, B. Zhang, L. J. Rajakovich, B. D. Allen, C. Krebs, A. K. Boal and J. M. Bollinger, Hydrogen Donation but not Abstraction by a Tyrosine (Y68) during Endoperoxide Installation by Verruculogen Synthase (FtmOx1), *J. Am. Chem. Soc.*, 2019, **141**(25), 9964–9979.
9 L. Wu, Z. Wang, Y. Cen, B. Wang and J. Zhou, Structural Insight into the Catalytic Mechanism of the Endoperoxide Synthase FtmOx1, *Angew. Chem., Int. Ed.*, 2022, **61**(12), e202112063.
10 C.-Y. Lin, A. L. Muñoz Hernández, T. N. Laremore, A. Silakov, C. Krebs, A. K. Boal and J. M. Bollinger, , Jr., Use of Noncanonical Tyrosine Analogues to Probe Control of Radical Intermediates during Endoperoxide Installation by Verruculogen Synthase (FtmOx1), *ACS Catal.*, 2022, **12**(12), 6968–6979.
11 T. Mori, R. Zhai, R. Ushimaru, Y. Matsuda and I. Abe, Molecular insights into the endoperoxide formation by Fe(II)/α-KG-dependent oxygenase NvfI, *Nat. Commun.*, 2021, **12**(1), 4417–4427.
12 Y. Matsuda, T. Awakawa, T. Wakimoto and I. Abe, Spiro-ring formation is catalyzed by a multifunctional dioxygenase in austinol biosynthesis, *J. Am. Chem. Soc.*, 2013, **135**(30), 10962–10965.
13 Y. Matsuda, T. Iwabuchi, T. Fujimoto, T. Awakawa, Y. Nakashima, T. Mori, H. Zhang, F. Hayashi and I. Abe, Discovery of Key Dioxygenases that Diverged the Paraherquonin and Acetoxydehydroaustin Pathways in Penicillium brasilianum, *J. Am. Chem. Soc.*, 2016, **138**(38), 12671–12677.
14 Y. Nakashima, T. Mori, H. Nakamura, T. Awakawa, S. Hoshino, M. Senda, T. Senda and I. Abe, Structure function and engineering of multifunctional non-heme iron dependent oxygenases in fungal meroterpenoid biosynthesis, *Nat. Commun.*, 2018, **9**(1), 104.
15 Y. Matsuda, T. Wakimoto, T. Mori, T. Awakawa and I. Abe, Complete biosynthetic pathway of anditomin: nature's sophisticated synthetic route to a complex fungal meroterpenoid, *J. Am. Chem. Soc.*, 2014, **136**(43), 15326–15336.
16 Y. Nakashima, T. Mitsuhashi, Y. Matsuda, M. Senda, H. Sato, M. Yamazaki, M. Uchiyama, T. Senda and I. Abe, Structural and Computational Bases for Dramatic Skeletal Rearrangement in Anditomin Biosynthesis, *J. Am. Chem. Soc.*, 2018, **140**(30), 9743–9750.
17 K. Liu, J. Zhang, G. Zhang, L. Zhang, Z. Meng, L. Ma, W. Zhang, W. Xiong, Y. Zhu, B. Wang and C. Zhang, Deciphering Deoxynybomycin Biosynthesis Reveals Fe(II)/α-Ketoglutarate-Dependent Dioxygenase-Catalyzed Oxazoline Ring Formation and Decomposition, *J. Am. Chem. Soc.*, 2023, **145**(50), 27886–27899.
18 N. Steffan, A. Grundmann, S. Afiyatullov, H. Ruan and S. M. Li, FtmOx1, a non-heme Fe(II) and alpha-ketoglutarate-dependent dioxygenase, catalyses the endoperoxide formation of verruculogen in Aspergillus fumigatus, *Org. Biomol. Chem.*, 2009, **7**(19), 4082–4087.
19 M. Bu, B. B. Yang and L. Hu, Natural Endoperoxides as Drug Lead Compounds, *Curr. Med. Chem.*, 2016, **23**(4), 383–405.
20 W. L. Smith, D. L. DeWitt and R. M. Garavito, Cyclooxygenases: structural, cellular, and molecular biology, *Annu. Rev. Biochem.*, 2000, **69**, 145–182.
21 M. A. Johnson and R. Croteau, Biosynthesis of ascaridole: iodide peroxidase-catalyzed synthesis of a monoterpene endoperoxide in soluble extracts of Chenopodium ambrosioides fruit, *Arch. Biochem. Biophys.*, 1984, **235**(1), 254–266.
22 N. G. Sharaf and A. M. Gronenborn, (19)F-modified proteins and (19)F-containing ligands as tools in solution NMR studies of protein interactions, *Methods Enzymol.*, 2015, **565**, 67–95.
23 Y. Yu, Q. Zhou, L. Wang, X. Liu, W. Zhang, M. Hu, J. Dong, J. Li, X. Lv, H. Ouyang, H. Li, F. Gao, W. Gong, Y. Lu and J. Wang, Significant improvement aof oxidase activity through the genetic incorporation of a redox-active unnatural amino acid, *Chem. Sci.*, 2015, **6**(7), 3881–3885.
24 F. Li, P. Shi, J. Li, F. Yang, T. Wang, W. Zhang, F. Gao, W. Ding, D. Li, J. Li, Y. Xiong, J. Sun, W. Gong, C. Tian and J. Wang, A genetically encoded 19F NMR probe for tyrosine phosphorylation, *Angew. Chem., Int. Ed.*, 2013, **52**(14), 3958–3962.
25 W. Minor, M. Cymborowski, Z. Otwinowski and M. Chruszcz, HKL-3000: the integration of data reduction and structure solution–from diffraction images to an initial model in minutes, *Acta Crystallogr. D Biol. Crystallogr.*, 2006, **62**(Pt 8), 859–866.

26 A. J. McCoy, R. W. Grosse-Kunstleve, P. D. Adams, M. D. Winn, L. C. Storoni and R. J. Read, Phaser crystallographic software, *J. Appl. Crystallogr.*, 2007, **40**(Pt 4), 658–674.
27 P. Emsley, B. Lohkamp, W. G. Scott and K. Cowtan, Features and development of Coot, *Acta Crystallogr. D Biol. Crystallogr.*, 2010, **66**(Pt 4), 486–501.
28 P. V. Afonine, R. W. Grosse-Kunstleve, N. Echols, J. J. Headd, N. W. Moriarty, M. Mustyakimov, T. C. Terwilliger, A. Urzhumtsev, P. H. Zwart and P. D. Adams, Towards automated crystallographic structure refinement with phenix.refine, *Acta Crystallogr. D Biol. Crystallogr.*, 2012, **68**(Pt 4), 352–367.
29 D. Liebschner, P. V. Afonine, M. L. Baker, G. Bunkoczi, V. B. Chen, T. I. Croll, B. Hintze, L.-W. Hung, S. Jain, A. J. McCoy, N. W. Moriarty, R. D. Oeffner, B. K. Poon, M. G. Prisant, R. J. Read, J. S. Richardson, D. C. Richardson, M. D. Sammito, O. V. Sobolev, D. H. Stockwell, T. C. Terwilliger, A. G. Urzhumtsev, L. L. Videau, C. J. Williams and P. D. Adams, Macromolecular structure determination using X-rays, neutrons and electrons: recent developments in Phenix, *Acta Crystallogr. D Biol. Crystallogr.*, 2019, **75**(10), 861–877.
30 P. Schultz, Expanding the genetic code, *Protein Sci.*, 2023, **32**(1), e4488.
31 R. Cheng, R. Lai, C. Peng, J. Lopez, Z. Li, N. Naowarojna, K. Li, C. Wong, N. Lee, S. A. Whelan, L. Qiao, M. W. Grinstaff, J. Wang, Q. Cui and P. Liu, Implications for an imidazol-2-yl carbene intermediate in the rhodanase-catalyzed C-S bond formation reaction of anaerobic ergothioneine biosynthesis, *ACS Catal.*, 2021, **11**(6), 3319–3334.
32 D. Xie, M. Yu, R. T. Kadakia and E. L. Que, (19)F Magnetic Resonance Activity-Based Sensing Using Paramagnetic Metals, *Acc. Chem. Res.*, 2020, **53**(1), 2–10.
33 Q. Miao, C. Nitsche, H. Orton, M. Overhand, G. Otting and M. Ubbink, Paramagnetic Chemical Probes for Studying Biological Macromolecules, *Chem. Rev.*, 2022, **122**(10), 9571–9642.
34 T. R. Alderson and L. E. Kay, NMR spectroscopy captures the essential role of dynamics in regulating biomolecular function, *Cell*, 2021, **184**(3), 577–595.
35 C. Y. Lin, A. L. Munoz, T. N. Laremore, A. Silakov, C. Krebs, A. K. Boal and J. M. Bollinger Jr, Use of Noncanonical Tyrosine Analogues to Probe Control of Radical Intermediates during Endoperoxide Installation by Verruculogen Synthase (FtmOx1), *ACS Catal.*, 2022, **12**(12), 6968–6979.
36 F. Wang, Y. Gao, C. Wang, W. Lan, J. Gan and C. Cao, Structure-based insights into mechanism of endoperoxidase FtmOx1 catalyzed reactions, *Catal. Sci. Technol.*, 2023, **13**, 6839–6849.